EPJ Web of Conferences **60**, 14006 (2013)
DOI: 10.1051/epjconf/20136014006

DØ Results on Diphoton Direct Production and Photon + b and c Jet Production

Lee Sawyer[1, a], on behalf of the DØ Collaboration

[1] *Louisiana Tech University*

Abstract. In this note we present measurements of the direct photon pair production cross sections using 8.5 fb^{-1} of data collected with the DØ detector at the Fermilab Tevatron $p\bar{p}$ collider at $\sqrt{s}$ = 1.96 TeV. The results are shown as differential distributions with respect to the photon pair mass, pair transverse momentum, azimuthal angle, and polar scattering angle in the Collins-Soper frame. We also present measurements of the differential cross section $d\sigma/dp_T^{\gamma}$ for the inclusive production of a photon in association with a *b*- or *c*-quark jet. The results are based on 8.7 fb^{-1} of data, and the measured cross sections are compared with next-to-leading order perturbative QCD calculations using different sets of parton distribution functions as well as to predictions based on the kT-factorization QCD approach, and those from various Monte Carlo event generators.

1 Introduction

Direct photon production in hadron collisions provides a precise probe of perturbative Quantum Chromodynamics (pQCD), particularly as a test of soft gluon resummation. Diphoton production can proceed through Born-level and box diagrams in pQCD, as well as single or double parton fragmentation. In addition, high mass diphoton pairs form a major irreducible background to searches for Higgs boson production via the $H \to \gamma\gamma$ decay channel. Therefore, the measurement of diphoton production cross sections at the Tevatron collider is important for both comparisons to QCD as well as for search for the Higgs or new phenomena producing diphoton resonances. In this note we present single differential cross-section for diphoton production, in bins of the diphoton invariant mass $M_{\gamma\gamma}$, total transverse momentum of the pair $p_T^{\gamma\gamma}$, and polar scattering angle $|\cos\theta^*|$ in the frame with no net transverse momentum (computed as $\cos\theta^* = \tanh(\eta_1 - \eta_2)/2$). We also compare diphoton production for the cases of small and large opening angles between the two photons.

Photon plus jet events can also be used as a probe of the partonic structure of the protons and antiprotons. Measurement of the production of isolated photons in association with jets initiated by *b*- or *c*-type quarks can provide a test of the Parton distribution Functions (PDFs) of these quark species in the colliding hadrons.

The data presented were taken in $p\bar{p}$ collisions at a center-of-mass energy of $\sqrt{s}$ = 1.96 TeV, collected with the DØ detector, a detailed description of which can be found in Ref. [1]. We select events with photons with calorimeter and track isolations and also satisfying shower shape cuts based on the calorirmeter and CPS. Please see details in [2] and [3]. Jets are defined by the Run II midpoint cone jet algorithm [4] with a cone radius of $R_{\rm cone} = \sqrt{(\Delta y)^2 + (\Delta\phi)^2} = 0.7$ in rapidity y and azimuthal angle ϕ.

2 Direct Diphoton Production

The data used in this analysis were collected using a combination of triggers requiring at least two clusters of energy in the EM calorimeter with loose shower shape requirements and varying p_T thresholds between 15 GeV and 25 GeV, and correspond to an integrated luminosity of 8.5 ± 0.5fb^{-1}. The two photons had to have $p_T > 18$ and 17 GeV and be with $|\eta| < 0.9$ and a separation of $\Delta R(\gamma\gamma) > 0.4$. An artificial neural network was applied to further reject jet backgrounds; see [3] for additional details, as well as estimates of backgrounds, uncertainties, and details of the theoretical comparisons.

Cross sections were calculated as $\frac{d\sigma}{dX} = \frac{N_{\gamma\gamma}}{\epsilon \times A \times L \times \Delta_X}$ where X represents the kinematical variable being studies ($M_{\gamma\gamma}$, $p_T^{\gamma\gamma}$, $\Delta\phi^{\gamma\gamma}$, $|\cos\theta^*|$) and Δ_X is the bin width in this variable. The event selection efficiency ϵ, acceptance A, and integrated L, along with the background estimation on the number of diphoton events $N_{\gamma\gamma}$ contribute a total systemic uncertainty of around +15/-12%, relatively flat over most of the $M_{\gamma\gamma}$ range.

Single differential cross section are shown in Figures 1 and 2. The experimental measurements are compared to theoretical predictions based on the SHERPA [5], DIPHOX [6], and RESBOS [7] Monte Carlos using the CTEQ6.6M [8] PDFs; and 2γNNLO [9] Monte Carlo using the MSTW2008NNLO [10] PDFs. PDF uncertainties were computed with DIPHOX with the CTEWQ6.6M eigenvectors. Each were run with $\mu_R = \mu_F = \mu_f = M_{\gamma\gamma}$.

a. e-mail: sawyer@phys.latech.edu

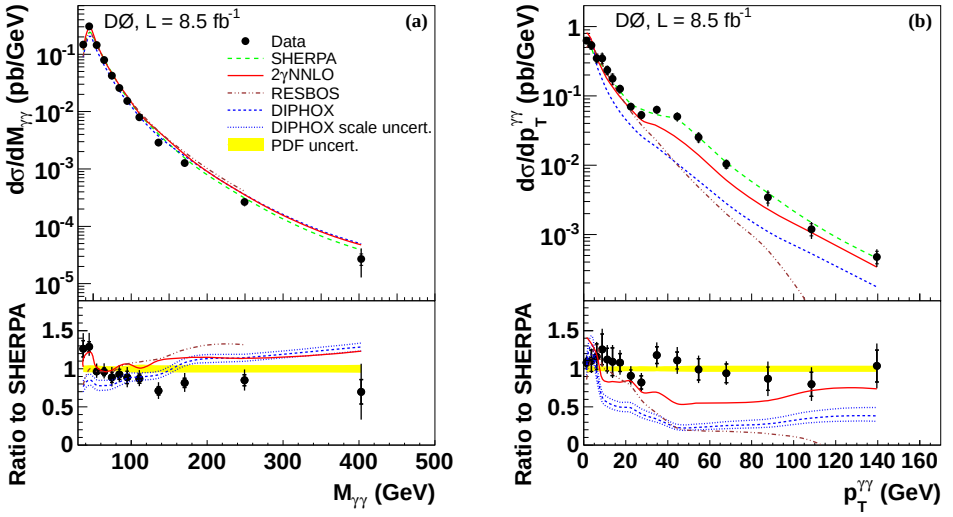

Figure 1. (left) The diphoton cross section as a function of the invariant mass $M_{\gamma\gamma}$ of the photon pair. (right) The diphoton cross section as a function of the transverse momentum $p_T^{\gamma\gamma}$ of the photon pair. Error bars include systematic uncertainties for both plots.

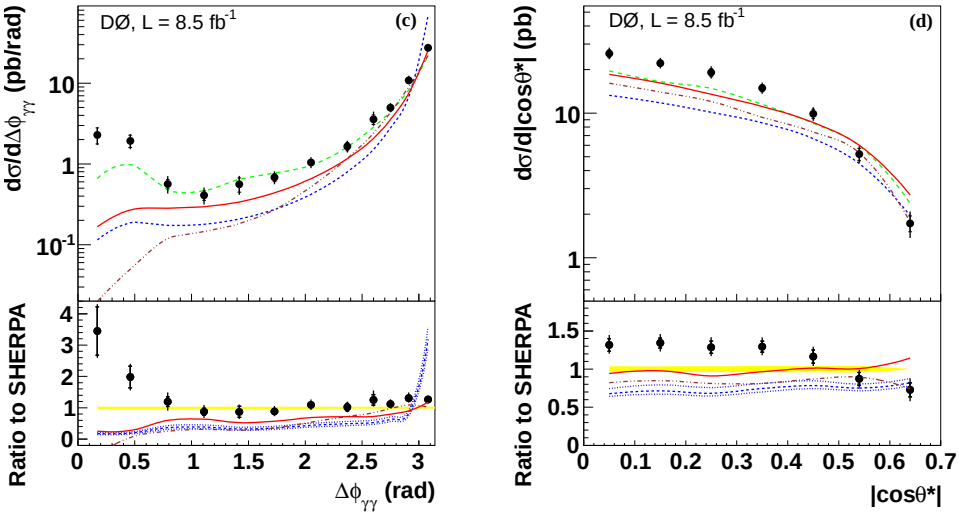

Figure 2. (left)The diphoton cross section as a function of the azimuthal opening angle $\Delta\phi^{\gamma\gamma}$ of the photon pair. (right) The diphoton cross section as a function of the scattering angle $|\cos\theta^*|$ of the photon pair. Error bars include systematic uncertainties for both plots.

Double differential cross section are formed in two bins bins of the diphoton azimuthal opening angle $\Delta\phi^{\gamma\gamma}$: $\Delta\phi^{\gamma\gamma} < \frac{\pi}{2}$ and $\Delta\phi^{\gamma\gamma} > \frac{\pi}{2}$. Figures 3 and 4 show the the cross sections for $M_{\gamma\gamma}$, $p_T^{\gamma\gamma}$, and $|\cos\theta^*|$ in the two $\Delta\phi^{\gamma\gamma}$ bins.

3 Photon + b-Jet Cross Section

The production of an isolated photon in association with a b-quark provides important tests of Quantum Chromodyamics, and can yield information about the b-quark and gluon PDFs. For low p_T photons, production is dominated by the Compton-like scattering of a gluon ($gb \to \gamma b$), while for photons with $p_T \geq 70$ GeV quark-antiquark annihilation $q\bar{q} \to \gamma g \to \gamma b\bar{b}$ dominates. Photons may also be produced in quark or gluon fragmentation, but this is suppressed by requiring the photon to be isolated.

We measure the $\gamma + b$-jet cross section as a function of the p_T^{γ} of the isolated photon, with $30 < p_T^{\gamma} < 300$ GeV for photons in $|y^{\gamma}| < 1.0$ (central) and $30 < p_T^{\gamma} < 200$ GeV for $1.5 < |y| < 2.5$ (forward). The b-jets are required to have $|y^{jet}| < 1.5$ and $p_T^{jet} > 15$ GeV. Jets initiated by light quarks are suppressed using a dedicated artificial neural network for b-jet identification. The fraction of b-jets is calculated by fitting templates of the invariant mass distributions of tracks associated with the secondary vertex (M_{SV}); see figure 5. Please refer to [2] for analysis details,

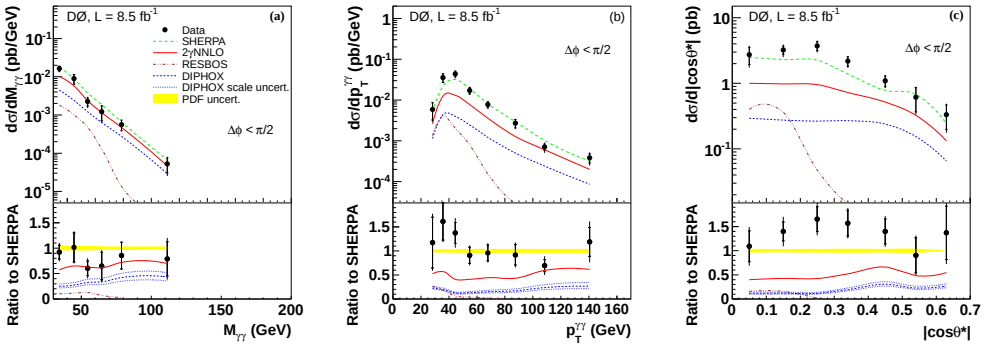

Figure 3. The diphoton cross section as a function of the transverse momentum $M_{\gamma\gamma}$, $p_T^{\gamma\gamma}$, and $|\cos\theta^*|$ of the photon pair, for photon pairs with $\Delta\phi^{\gamma\gamma} < \frac{\pi}{2}$. Error bars include systematic uncertainties.

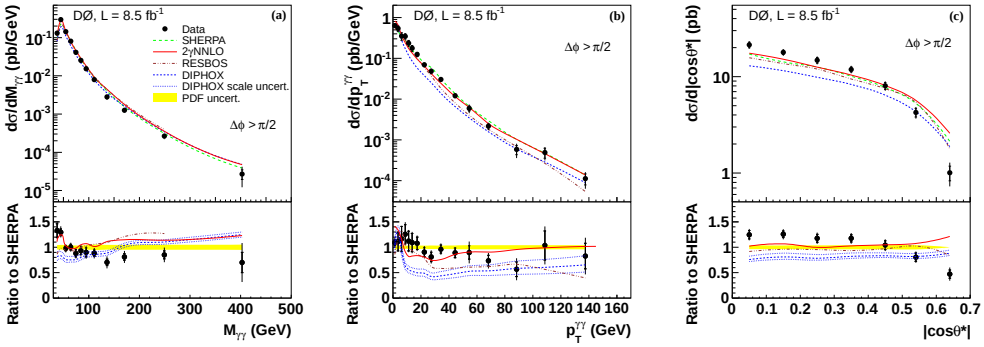

Figure 4. The diphoton cross section as a function of the transverse momentum $M_{\gamma\gamma}$, $p_T^{\gamma\gamma}$, and $|\cos\theta^*|$ of the photon pair, for photon pairs with $\Delta\phi^{\gamma\gamma} > \frac{\pi}{2}$. Error bars include systematic uncertainties.

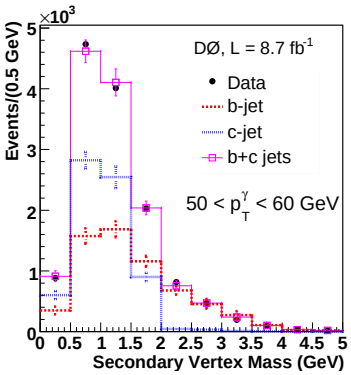

Figure 5. (Distribution of secondary vertex mass after all selection criteria for a representative bin of $50 < p_T < 60$ GeV. The expected contribution from the light-jet component has been subtracted from the data. The distributions for the b-jet and c-jet templates (with statistical uncertainties) are shown normalized to their respective fitted fractions.

estimates of uncertainties, and details of the comparison to theoretical predictions.

In figure 6 we show the measured cross section for $\gamma + b$-jet production as a function of p_T^{γ}. along with theoretical predictions. The uncertainties on the data points include statistical and systematic contributions added in quadrature.

In the figure 7 the ratio of data to the NLO pQCD predictions are shown. The uncertainties on the data include both statistical (inner error bar) and full uncertainties (entire error bar).

4 Photon + c-jet Cross Section

In a similar fashion to the $\gamma + b$ analysis, we can also extract the fraction of c-quark jets from the liklihood template fits to the M_{SV} distribution. This allows us to measure the cross section of $\gamma + c$-jets production as a function of p_T^{γ}. Please see [14] for complete analysis details. Figure 8 shows the resulting cross section measurement for $\gamma + c$-jet events, while figure 9 shows the ratio of the measured cross sections of $\gamma + c$-jet events to $\gamma + b$-jet events as a function of p_T^{γ}. The uncertainties on the data points include statistical and systematic contributions added in quadrature. In both plots, comparisons are made to pQCD and kT-factorization calculations as well as Monte Carlo generator predictions.

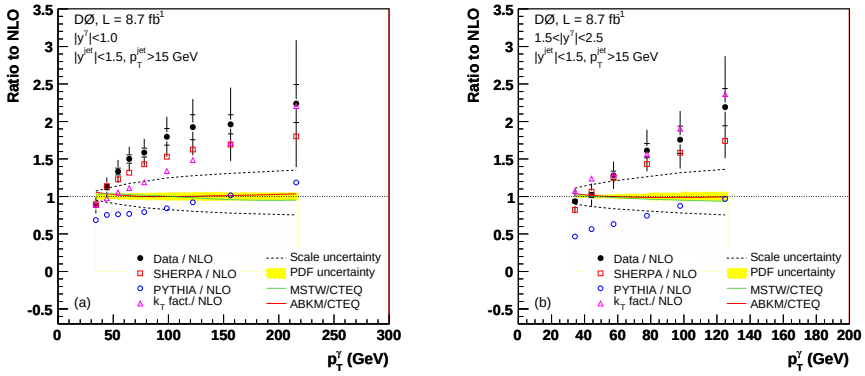

Figure 7. The ratio of $\gamma + b$ production differential cross sections between data and NLO QCD predictions with uncertainties for the rapidity regions $|y| < 1.0$ (a) and $1.5 < |y| < 2.5$ (b). Also shown are the uncertainties on the theoretical QCD scales and the CTEQ6.6M PDFs. The ratio of NLO predictions with CTEQ6.6M to those with MSTW2008 and ABKM09NLO [13] are also shown.

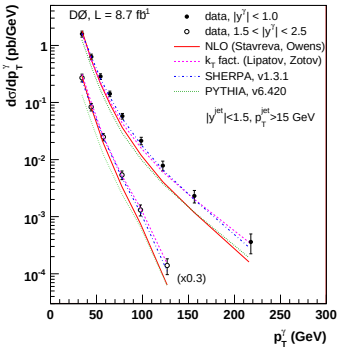

Figure 6. The $\gamma + b$ production differential cross sections as a function of p_T in the two photon rapidity regions, $|y| < 1.0$ and $1.5 < |y| < 2.5$ (the latter results are multiplied by 0.3 for presentation). The measurements are compared to the NLO QCD calculations [11] using CTEQ6.6M PDFs (solid line). The predictions from SHERPA, PYTHIA and a "kT factorization" approach [12] are shown by the dash-dotted, dotted and dashed lines, respectively.

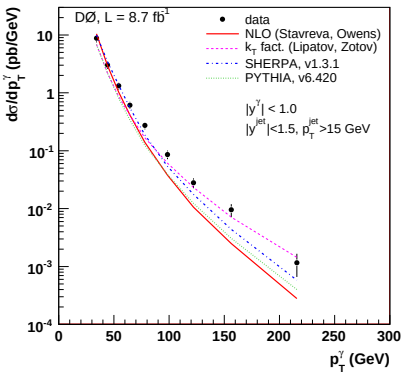

Figure 8. The $\gamma + c$-jet differential production cross sections as a function of p_T. The horizontal error bars show the p_T bins. The measurements are compared to the NLO QCD calculations using CTEQ6.6M PDFs (solid line). The predictions from SHERPA, PYTHIA, and "kT factorization" approach are shown by the dash-dotted, dotted and dashed lines, respectively.

References

[1] V. M. Abazov *et al.* (D0 Collaboration), Nucl. Instrum. Methods Phys. Res. A **565**, 463 (2006).

[2] V. M. Abazov *et al.* (D0 Collaboration), Phys. Lett. B **714**, 32 (2012)

[3] V. M. Abazov *et al.* (D0 Collaboration), Accepted by Phys. Lett. B, arXiv:1301.4536

[4] G. C. Blazey *et al.*, in: U. Baur, R.K. Ellis, and D. Zeppenfeld (Eds.), *Proceedings of the Workshop: QCD and Weak Boson Physics in Run II,* Fermilab-Pub-00/297 (2000).

[5] T. Gleisberg, *et al.*, J. High Energy Phys. 02, 007 (2009). We use sherpa v.1.2.2.

[6] T. Binoth, J. Ph. Guillet, E. Pilon, and M. Werlen, Eur. Phys. J. C **16**, 311 (2000).

[7] C. Balazs, E. L. Berger, P. Nadolsky, and C.-P. Yuan, Phys. Rev D **76**, 013009 (2007).
P. Nadolsky, C. Balazs, E. Berger, C.-P. Yuan, Phys. Rev. D **76**, 013008 (2007).
C. Balazs, E. Berger, S. Mrenna, and C.-P. Yuan, Phys. Rev. D **57**, 6934 (1998).

[8] J. Pumplin, *et al.*, J. High Energy Phys. **0207**, 012 (2002) and D. Stump et al., J. High Energy Phys. **0310**, 046 (2003).

[9] S. Catani, L. Cieri, D. Florian, G. Ferrera, and M. Grazzini, Phys. Rev. Lett. **108**, 072001 (2012).

[10] A. D. Martin, W. J. Stirling, R. S. Thorne, and G. Watt, Eur. Phys. J. C **63**, 189 (2009).

[11] T. Stavreva and J.F. Owens, Phys. Rev. D **79**, 054017 (2009).

[12] A.V. Lipatov and N.P. Zotov, J. Phys. G 34, 219 (2007) and S.P. Baranov, A.V. Lipatov, and N.P. Zotov, Eur. Phys. J. C 56, 371 (2008).

[13] S. Alekhin et al., Phys. Rev. D **81**, 014032 (2010).

[14] V. M. Abazov *et al.* (D0 Collaboration), Phys. Lett. B **719**, 354 (2013).

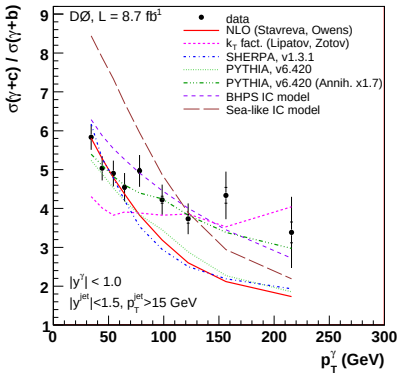

Figure 9. The ratio of $\gamma + c$-jet events to $\gamma + b$-jet prodction cross sections for data along with theoretical predictions, as a function of p_T^{γ}.